Dynamics of vortex nucleation in ^{3}He-A flow

N. B. Kopnin,* P. I. Soininen, and M. M. Salomaa†
Low Temperature Laboratory, Helsinki University of Technology, SF-02150 Espoo, Finland
(Received 26 November 1990)

Quantum phase slippage in superfluid ^{3}He flow is simulated numerically in rectangular slab geometries. Assuming that the flow is confined to a channel having horizontal surfaces close to each other, the spatial problem reduces to the two transverse dimensions; we report time-dependent computer simulations of superfluid ^{3}He flow in 2+1 dimensions using the time-dependent Ginzburg-Landau equations. The quantum-dynamic processes of phase slippage in ^{3}He are demonstrated to be associated with superfluid vortex nucleation; we thus confirm Anderson's assumption for phase slippage through vortex motion in superfluids. We also find several other phase-slip scenarios involving vortices, phase-slip lines, and combinations thereof for the coupled multicomponent order-parameter amplitudes. We consider both diffuse and specular boundary conditions at the side walls and demonstrate that our results are essentially independent of the boundaries. We compute the critical current for vortex nucleation as a function of the channel width, and compare it with existing theories of vortex nucleation; we also discuss our calculations in connection with experiments on phase slippage in ^{3}He flow. One of our most important results is that the superfluid order parameter for the vortices generated in the computer simulations does not vanish anywhere; i.e., the vortices possess superfluid core structures; hence the processes of phase slip for superfluid ^{3}He are nonlocal in space-time.

I. INTRODUCTION

Quantized vortices in superfluids form in rotating cryostats and also in flows at sufficiently high velocity. However, dynamics of the nucleation for quantized vortices in all known superfluid systems is still far from being well understood.[1] In the case of flow, the general picture is that vortex motion enables phase slippage which, according to Anderson,[2] is necessary in order to account for the dissipation.

For superfluid ^{3}He, there presently exist several experimental verifications that vortices can, indeed, be created by flow. Vortices were created in bulk ^{3}He in early experiments[3] due to the superfluid counterflow owing to a temperature gradient.[4,5] Vortex formation has also been observed in recent experiments[6] on the flow of ^{3}He through a narrow slit with dimensions on the order of the coherence length.

One of the most prominent contrasts between vortex formation in bulk ^{3}He and that in its flow through narrow channels occurs in the A phase. It is well established that the so-called continuous vortices can be formed in bulk ^{3}He-A; these smooth structures possess the A-phase order parameter even down to the center of the vortex. These vortices do not feature a normal core, and the finite (even) number of circulation quanta are produced by a texture of the anisotropy vector $\boldsymbol{l}$ (for reviews, see, e.g., Refs. 7 and 8). The orbital dynamics of $\boldsymbol{l}$ and the formation of continuous vortices have been considered in a one-dimensional flow field.[9,10]

However, the anisotropy vector $\boldsymbol{l}$ tends to be fixed in a channel of restricted geometry, whence the formation of continuous vortices is impossible. Therefore, one would expect singular vortices to occur in this situation; in particular, there arises the question whether vortices with a normal core will be formed in such a channel (as in superconductors) or if there is still the possibility for the formation of superfluid-core vortices,[11] as in bulk ^{3}He.

The goal of the present paper is to study the dynamics of the phase-slippage process, and the structure of vortices formed by a flow of superfluid ^{3}He-A through a channel with transverse dimensions on the order of the superfluid coherence length, $\xi(T)$. We also investigate the possibility for superfluid-core vortices to be formed in restricted geometries. Preliminary results of this work have been published in Letter format.[12]

Employing computer simulations of the time-dependent Ginzburg-Landau (TDGL) equations, we find that, depending on the channel size, the phase-slip processes in the flow of ^{3}He-A can be quite versatile; they occur through the formation of vortices and/or phase-slip lines (PSL: a line of zeroes of the order parameter) for one or several components of the multicomponent order parameter. The general feature of the phase-slip solutions obtained is that the components of the order parameter never vanish simultaneously, thus proving the existence of superfluid-core vortices in the flow of ^{3}He-A through narrow channels. Phase-slip centers with superfluid cores have recently also been found for one-dimensional flows of ^{3}He through narrow channels.[13]

The absence of a normal core constitutes the main difference between phase slippages in superfluid ^{3}He, with its multicomponent order parameter, and in He II or in superconductors, where phase slippage is due to normal-core vortices or phase-slip centers at which the order parameter turns to zero periodically. For superconductors, phase-slip processes have been studied extensively—experimentally and theoretically—for nar-

row filaments with transverse sizes on the order of the coherence length (see the review[14] and references therein); recently computer simulations of vortex formation have also been made for superconductors in a two-dimensional geometry.[15]

In Sec. II we discuss the model used in our computations. In particular, we describe the channel geometry and its relation to the existing experimental arrangement of Ref. 6. We also discuss the mathematical background, i.e., the TDGL model, its relevance, and its regime of applicability. Simplifications adopted for the calculation are also explained. In Sec. III we present our results. The physical picture of phase slippage, the critical current, vortex formation and structure, and the relation between our results and experiments are discussed in Sec. IV.

II. THEORETICAL MODEL

A. Superflow geometry

For theoretical studies using numerical simulation, the specific geometry and symmetry of the flow channel is quite essential; its shape and dimensions strongly affect the structure of the order parameter $A_{\alpha i}$ in superfluid ^{3}He. For example, in a narrow cylindrical channel with radius on the order of $\xi(T)$, only one of the three orbital spin-dependent complex order-parameter components $A_{\alpha i}$ would survive (α and i refer to the spin and orbital degrees of freedom, respectively). In this case the single nonvanishing amplitude would be $A_{\alpha z}$, where z is directed along the channel, and one would lose the characteristic distinction of superfluid ^{3}He as a system possessing a multicomponent order parameter—in comparison with other superfluids with only one-component order parameters.

In the present paper we restrict ourselves to the study of ^{3}He states, which are close to the superfluid A phase. To preserve the characteristic A-phase-like structure of the order parameter in narrow channels, the simplest nontrivial flow situation to consider is slab geometry: a rectangular cross-section of width w, considerably larger than the height h. The length L of the channel may be arbitrary. For h on the order of the coherence length, the anisotropy vector $\boldsymbol{l}$ is fixed perpendicular to the horizontal surfaces of the channel. In the coordinate system chosen, see Fig. 1, with the z axis along the channel and y upwards, $A_{\alpha x}$ and $A_{\alpha z}$ are the only finite components of the order parameter. The cross-sectional configuration is chosen to resemble that employed in the experiments,[6] where the dimensions were $h = 0.3$ μm, and $w = 5$ μm, which correspond to $h \simeq 5, \ldots, 25\,\xi_s$, and $w \simeq 80$–$400\,\xi_s$, depending on the pressure [cf. Eq. (4)].

One can gain some understanding of the behavior of a superfluid flowing through a channel in the presence of a small pressure difference between its ends by using the so-called current-phase relation

$$j_s = j_c f(\delta\varphi)\,, \tag{1}$$

where j_s is the supercurrent and $\delta\varphi$ is the phase difference between the ends of the channel (see, e.g., Ref. 16). Since $\partial\varphi/\partial t \propto \mu$ in the bulk liquid, where μ is the chemical potential, the phase difference $\delta\varphi$ grows in time, and j_s will oscillate just as in the ac-Josephson effect. If the function $f(\delta\varphi)$ is multivalued, as one should expect for sufficiently long channels, the evolution of the phase difference ought to result in jumps for j_s from one branch of $f(\delta\varphi)$ to another. These discontinuities are connected with passages of vortices across the flow channel, which, in the time scale for which Eq. (1) is valid, happen instantaneously.

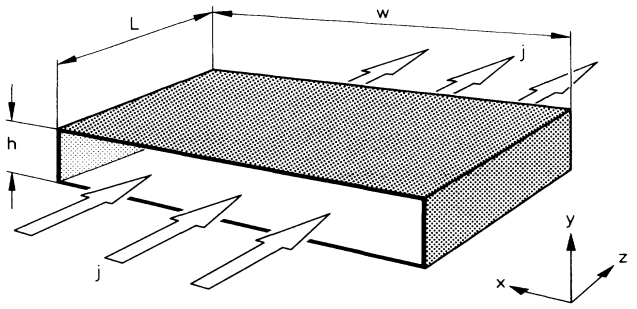

FIG. 1. Schematic illustration for the model "matchbox" geometry of the superfluid ^{3}He flow channel considered in this paper. In order to correspond to available experiments, the channel is here taken to be a wide rectangular slit of height h, width w, and length L. In the numerical simulations, a total constant current j (indicated by the large arrows in this figure) is imposed along z.

In spite of its usefulness, Eq. (1) cannot provide any information on how vortices are actually formed, and what their structure and dynamics are, since due to its very nature the adiabatic approximation used for the derivation of Eq. (1) necessarily breaks down just when the instability for vortex formation appears. Moreover, a vortex in the presence of flow cannot be stationary; it should move under the Magnus force. Therefore, one needs to use dynamic—not static—equations in order to study vortex formation and the time-dependent vortex structures in superfluid flows.

B. Dynamic equations

The general set of dynamic equations for superfluid ^{3}He includes an equation for the order parameter $A_{\alpha i}(x,y,z;t)$, a generalized kinetic equation for the quasiparticle distribution function, and also an expression for the current produced by both the superfluid and normal components. However, it is very difficult—if at all possible—to write down a closed set of equations containing only the order parameter for an unrestricted situation, even using the relatively simple microscopic BCS theory. The principal obstacle is the difficulty of deriving a general expression for the quasiparticle excitation spectrum for situations where spatial variations of the or-

der parameter occur on the scale of the coherence length, $\xi(T)$.

Therefore, it seems reasonable to employ a simple model system of dynamic equations that is capable of describing nonadiabatic processes for spatially varying distributions of the order parameter. The time-dependent Ginzburg-Landau (TDGL) equations provide one such description. This approach differs from the hydrodynamic and Lagrangian methods[17] in that it takes into account the dissipation caused by order-parameter relaxation, which is clearly of great importance for processes involving the creation and motion of vortices, in particular. We now turn to discuss the TDGL equations in more detail in connection with superfluid phase slippage in ^{3}He flow.

The total mass current in the channel is the sum total of the superfluid ($\mathbf{j}^{(s)}$) and normal ($\mathbf{j}^{(n)}$) components:

$$\mathbf{j} = \mathbf{j}^{(n)} + \mathbf{j}^{(s)} . \tag{2}$$

The Ginzburg-Landau expression for the supercurrent is[18]

$$j_i^{(s)} = \frac{2}{5}\frac{N(0)m}{\hbar}\xi_s^2 [\, A_{\alpha n}^{\star}(-i\nabla_i A_{\alpha n}) + A_{\alpha n}^{\star}(-i\nabla_n A_{\alpha i}) + A_{\alpha i}^{\star}(-i\nabla_n A_{\alpha n}) + \text{c.c.}], \tag{3}$$

where $N(0) = mp_F/(2\pi^2\hbar^3)$ is the density of ^{3}He states per one spin projection, and

$$\xi_s^2 \equiv \frac{7\zeta(3)\hbar^2 v_F^2}{48\pi^2 T_c^2} \tag{4}$$

is the characteristic coherence length. The order parameter $A_{\alpha i}$ is defined through $\hat{\Delta}_p = i\hat{\sigma}^{(\alpha)}\hat{\sigma}^{(2)}A_{\alpha i}p_i$, where $|\Delta_p|$ is the energy gap for spatially uniform $A_{\alpha i}$.

The normal current through a narrow channel whose transverse dimensions are less than the mean free path for mutual quasiparticle collisions, ℓ, is determined by the ^{3}He quasiparticle scattering at the walls. For diffuse processes,[19]

$$j_z^{(n)} = -2mN(0)\mathcal{D}\frac{\partial\mu}{\partial z} , \tag{5}$$

where $\mathcal{D}$ is the diffusion coefficient. For a rectangular channel with $w \gg h$, $\mathcal{D}$ is given by

$$\mathcal{D} = \frac{v_F h}{4}\ln\left(\frac{w}{h}\right) ; \tag{6}$$

μ is constant over the channel cross-section in Knudsen flow.

The time-dependent equations for the order parameter $A_{\alpha i}$ in the weak-coupling approximation can be written in the form

$$-\tau\left(\frac{\partial}{\partial t} + \frac{2i}{\hbar}\mu\right)A_{\alpha i} + \frac{T_c - T}{T_c}A_{\alpha i} + \frac{3}{5}\xi_s^2(\delta_{ik}\nabla^2 + 2\nabla_i\nabla_k)A_{\alpha k} - \frac{7\zeta(3)}{40\pi^2 T_c^2}(2A_{\alpha i}A_{\beta k}^{\star}A_{\beta k} + 2A_{\alpha k}A_{\beta k}^{\star}A_{\beta i} + 2A_{\alpha k}A_{\beta i}^{\star}A_{\beta k} - 2A_{\beta i}A_{\alpha k}^{\star}A_{\beta k} - A_{\beta k}A_{\alpha i}^{\star}A_{\beta k}) = 0. \tag{7}$$

Here the time derivative of the order parameter occurs in conjunction with the chemical potential in accordance with gauge invariance. This serves to ensure that in equilibrium[2] one has $\partial\varphi/\partial t + 2\mu/\hbar = 0$. In Eq. (7), the chemical potential is measured with respect to the Fermi energy. The characteristic time τ in the TDGL theory is on the order of $\hbar/T_c$.

C. Units; reduced equations

For the numerical computations, it proves convenient to use dimensionless units as follows: let us present the order parameter in the form

$$A_{\alpha i} = \Delta a_{\alpha i} , \tag{8}$$

where

$$\Delta = \frac{40\pi^2(T_c - T)T_c}{7\zeta(3)} . \tag{9}$$

We measure distances in units of the transverse (T) temperature-dependent GL coherence length[18]

$$\xi_T(T) \equiv \sqrt{\frac{3}{5}}\xi_s\left(\frac{T_c - T}{T_c}\right)^{-1/2} , \tag{10}$$

and currents in units of

$$j_0 = \frac{2\sqrt{5}N(0)m\hbar v_F^2}{3\sqrt{3}\xi_s}\left(\frac{T_c - T}{T_c}\right)^{3/2} . \tag{11}$$

For the time scale we use the unit

$$t_0 = \frac{3\mathcal{D}}{2v_F^2}\left(\frac{T_c - T}{T_c}\right)^{-1} , \tag{12}$$

while the chemical potential is measured in $\mu_0 = \hbar/2t_0$. For clarity, convenience of the reader, and an easy reference, the units of length, ξ_s, and current, $j_0(1 - T/T_c)^{-3/2}$, employed in the present paper are displayed in Fig. 2 as functions of pressure.

In these units the normal component of the current in Eq. (2) is given by

$$j_z^{(n)} = -\frac{\partial\mu}{\partial z} , \tag{13}$$

while the supercurrent is

$$j_i^{(s)} = \tfrac{1}{2}\Big[\, a^*_{\alpha k}(-i\nabla_i a_{\alpha k}) + a^*_{\alpha k}(-i\nabla_k a_{\alpha i}) + a^*_{\alpha i}(-i\nabla_k a_{\alpha k}) + \text{c.c.}\Big], \tag{14}$$

and the order parameter satisfies the equation

$$-u\left(\frac{\partial}{\partial t} + i\mu\right) a_{\alpha k} + a_{\alpha k} + \delta_{kn}(\nabla^2 + 2\nabla_k\nabla_n) a_{\alpha n} - (2a_{\alpha k}a^*_{\beta n}a_{\beta n} + 2a_{\alpha n}a^*_{\beta n}a_{\beta k} + 2a_{\alpha n}a^*_{\beta k}a_{\beta n} - 2a_{\beta k}a^*_{\alpha n}a_{\beta n} - a_{\beta n}a^*_{\alpha k}a_{\beta n}) = 0. \tag{15}$$

Here u determines the ratio between the time scale t_0 and the characteristic time τ: $\tau/t_0 = (1 - T/T_c)u$. From Eq. (6) we get

$$u = \frac{2\tau v_F^2}{3\mathcal{D}} = \frac{8}{3}\frac{\tau v_F}{h\ln(w/h)}. \tag{16}$$

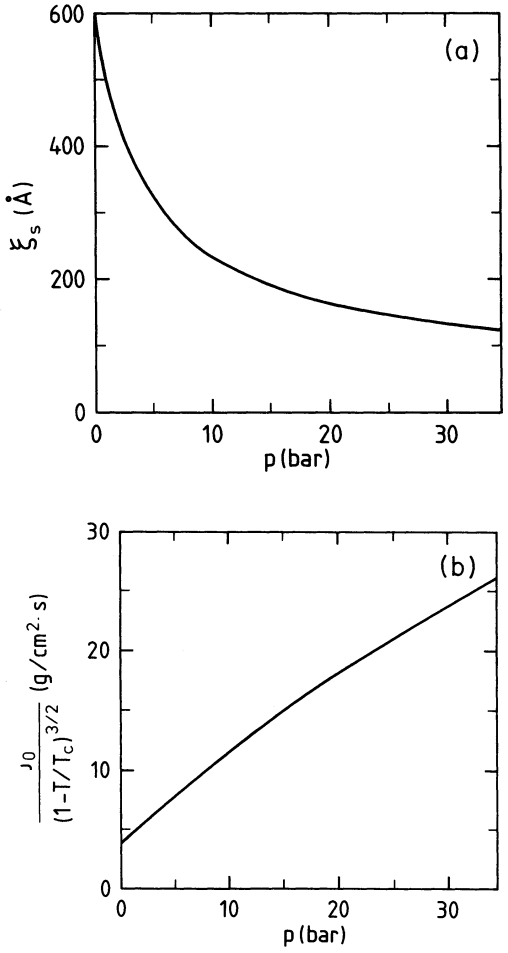

FIG. 2. Scales of (a) length, and (b) mass current used in this paper as functions of pressure. Numerical values were calculated using data from Refs. 20 and 8.

Since, in general, $\tau v_F/h \simeq \xi_s/h$, and $w \gg h$, the parameter u in our model is small, in contrast to the TDGL equations for the theory of superconductivity,[14] where $u \simeq 1$. In Eqs. (13)–(15), the only parameter that depends on the properties of the channel is u.

D. Limitations of the model

Note that the TDGL equation (7) can be derived from the microscopic BCS theory only for the gapless situation.[21] For superfluid ^{3}He this limit is relevant, for example, when the temperature is so close to T_c that $\Delta\tau_\varepsilon \ll 1$, where τ_ε is the quasiparticle mean-free time. Such a temperature region is very narrow, $1 - T/T_c \sim 10^{-4}$, and impractical from the experimental point of view. Moreover, $\xi(T) > l$ for these temperatures, and the Knudsen formula, Eqs. (5) and (6), with μ homogeneous over the channel cross section, is no longer valid. Therefore, we do not claim that Eqs. (5)–(7) need strictly be valid in the above-mentioned temperature regime.

On the other hand, the set of TDGL equations can, however, be derived quite rigorously from the microscopic BCS theory for other realizations of the gapless limit when strong pair breaking is produced by the diffuse scattering of quasiparticles at closely spaced parallel surfaces confining the superfluid ^{3}He. Here one needs the height h of the channel to be very close to the critical value $h_c = 0.212\hbar v_F/T_{c_0}$ (with T_{c_0} denoting the critical temperature in the bulk liquid) for which superfluidity becomes completely extinguished.[22] For $h \approx h_c$, the order-parameter components $A_{\alpha y} = 0$ and the components $A_{\alpha x}$ and $A_{\alpha z}$ are small in comparison with their values in the bulk liquid.

The TDGL equations have been derived[23] for this case; in dimensionless units they have the form of Eqs. (13)–(15), now with the characteristic scales

$$\Delta^2 = \frac{16\ln 2}{\beta}T_c(T_c - T), \quad \xi_T = \frac{\hbar v_F}{4\Delta\beta^{1/2}}, \tag{17}$$

$$j_0 = \frac{\pi N(0)p_F h\Delta^2}{64\,T_c\,\xi_T}, \quad t_0 = \frac{64T_c\mathcal{D}\hbar}{\pi v_F h\Delta^2}. \tag{18}$$

The critical temperature $T_c \sim T_{c_0}[(h - h_c)/h_c]$. The numerical constant $\beta \sim 1$ is defined in Ref. 23; here the parameter

$$u = \frac{\ln(\hbar v_F/Th)}{4\beta\ln(w/h)} \tag{19}$$

is also small.

For channels with $h \approx h_c$, Eqs. (14) and (15) are actually to be considered as averaged over the channel height (over y) with the weight function introduced by Kjäldman, Kurkijärvi, and Rainer,[22] and by one of the present authors;[23] hence the nonzero components $a_{\alpha x}$ and $a_{\alpha z}$ do not depend on y. We refer to a more detailed discussion[23] concerning the derivation of the TDGL equations in the gapless limit. Note that for this limit, the effective coherence length ξ_T from Eq. (17) is considerably larger than h_c; therefore, the condition

$h \ll w$ can be satisfied for $w \approx \xi_T$ as well. In our computations, we consider channels both with $w \approx \xi_T$ and with $w \gg \xi_T$. The case $w \approx \xi_T$ refers just to the gapless limit discussed above.

To conclude our exposition of the dynamic equations, we emphasize that the TDGL model described by Eqs. (13)–(15) investigated in this work should in general be considered as a model only, although this model can be fully justified microscopically for gapless superfluidity in a narrow channel with diffuse walls. Just like the Ginzburg-Landau theory for the bulk phases of superfluid ^{3}He has a broad regime of applicability extending beyond the rigorously justifiable one, we expect our time-dependent Ginzburg-Landau calculations to be indicative of generic dynamic behavior for superfluid ^{3}He flow in restricted geometries.

E. Relation to experiments

Experimentally, a superfluid flow through narrow channels can be studied under several different conditions. One of possible experimental setups is that (i) a pressure difference across the ends of the channel is measured for given mass flow; this was done in the experiments with micropores.[24] It is also possible to (ii) measure the mass flow for a given pressure difference. One can equally well (iii) specify an initial phase difference $\delta\varphi$ across the ends of the channel and monitor the mass flow as $\delta\varphi$ relaxes.

In the experiments of Ref. 6, a combination of conditions (ii) and (iii) was realized: an initial phase difference produced by the flow through an auxiliary bypass later relaxed through the formation of vortices in the presence of a pressure gradient. Under conditions (i) and (iii), the onset of dissipation and of phase slippage due to the formation and motion of vortices occurs for currents and phase differences above certain critical values. In case (ii), phase slippage starts at any nonzero pressure difference.

For the present work we use condition (i) with a given constant averaged current density $\mathbf{j}$, where $\mathbf{j} = j_z^{(n)} + \langle j_z^{(s)} \rangle$, and $\langle j_z^{(s)} \rangle$ denotes the z component of the superfluid mass current $\mathbf{j}^{(s)}$, averaged over the cross section of the channel.

For states of superfluid ^{3}He close to the A phase, we present the order parameter in the form

$$a_{\alpha i} = d_\alpha a_i \ , \tag{20}$$

where d_α is a unit vector in spin space. Since the characteristic scale of the flow channel problem is considerably shorter than the dipole length, $\xi_D \approx 10^3 \xi_s$, we may assume that $d_\alpha = \text{const}$. In the slab geometry the order parameter a_i possesses two complex components, a_x and a_z.

We assume that a_x and a_z do not depend on y. This condition is strictly valid for the case when the TDGL equations follow from the microscopic theory, as discussed above. For more general cases, one may consider the a_i as the order-parameter components averaged over y.

F. Boundary conditions

We employed both diffuse (D) and specular (S) boundary conditions for the order-parameter components a_i at the side walls for $x = \pm w/2$, as defined by the following conditions:

$$(S) \quad a_x(x = \pm w/2, z) = 0 \ , \quad \frac{\partial a_z(x = \pm w/2, z)}{\partial x} = 0 \ ,$$

and

$$(D) \quad a_x(x = \pm w/2, z) = 0 \ , \quad a_z(x = \pm w/2, z) = 0 \ .$$

As discussed above, the chemical potential μ is independent of y and x.

The boundary conditions along z can be formulated more conveniently in terms of the moduli (ρ_x, ρ_z) and phases (φ_x, φ_z) for each component:

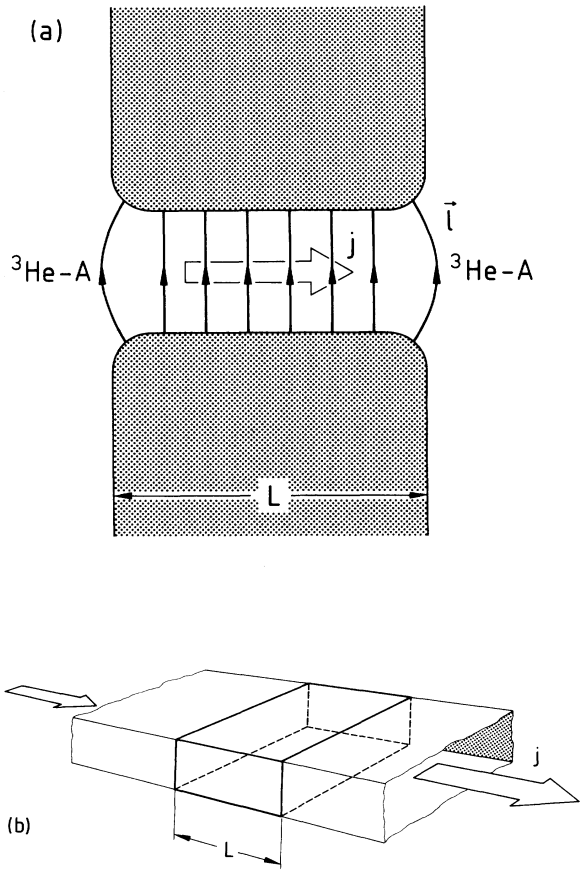

FIG. 3. Experimental physical realizations of the flow geometry considered: (a) a slit of length L, connecting two vessels of superfluid ^{3}He-A; solid arrows display the l-vector texture, open arrow represents the current flow, j; (b) a section, having length L, of a long flow channel with the current j passing through. Boundary conditions are periodic along the flow field.

$$a_x = \rho_x e^{i\varphi_x} , \quad a_z = \rho_z e^{i\varphi_z} . \tag{21}$$

At $z = 0$ and $z = L$ we require that

$$\varphi_z = \varphi_x + \frac{\pi}{2} + \pi k \quad (k \text{ is an integer}) , \tag{22}$$

$$\frac{\partial \rho_x}{\partial z} = \frac{\partial \rho_z}{\partial z} = 0 , \tag{23}$$

$$\frac{\partial \varphi_x}{\partial t} + \mu = \frac{\partial \varphi_z}{\partial t} + \mu = 0 . \tag{24}$$

Since μ is independent of x, Eqs. (22) and (24) are compatible. Equation (22) requires that the vectors Re(**a**) and Im(**a**) are to be perpendicular to each other at $z = 0$ and also at $z = L$ for the "pure" A phase, with $\rho_x = \rho_z$. The anisotropy vector $\boldsymbol{l} \propto \mathrm{Re}(\mathbf{a}) \times \mathrm{Im}(\mathbf{a})$ is directed upwards for an odd k and downwards for an even k.

The boundary conditions (22)–(24) correspond to two possible physical realizations: (a) a channel of length L, connecting two containers with ^{3}He in the A phase [it is assumed that the $\boldsymbol{l}$ vectors in both containers are parallel along y near the ends of the channel, see Fig. 3(a)] and (b) a long channel where superfluid ^{3}He is close to the A phase, and distributions of ρ_x, ρ_z, and $\mathbf{j}^{(s)}$ possess definite symmetry with respect to the lines $z = 0$ and L and repeat periodically along z; see Fig. 3(b).

In a long channel, Eqs. (22) to (24) are independent of the actual conditions at the ends of the channel; they are satisfied automatically on the lines $z = \text{const}$, about which the distributions of ρ_z, ρ_x, and $\mathbf{j}^{(s)}$ are symmetric. These boundary conditions coincide with the class 1 conditions for the one-dimensional flow[13] of ^{3}He and resemble those used for simulations of phase-slip processes in superconductors.[25]

III. PHASE-SLIP SOLUTIONS

We now consider numerical results for phase-slip solutions in superfluid ^{3}He.

A. Numerical scheme

Our numerical approach for solving the TDGL equations is that, for every time instant t, Eqs. (15) are solved with respect to the complex functions $a_x(x,z;t)$ and $a_z(x,z;t)$ with the chemical potential $\mu(z;t)$ integrated from

$$-\frac{\partial \mu(z;t)}{\partial z} = j - \langle j_z^{(s)} \rangle , \tag{25}$$

where the supercurrent

$$\langle j_z^{(s)} \rangle = \frac{1}{w} \int_{-w/2}^{+w/2} j_z^{(s)}(x,z;t)\, dx \tag{26}$$

is computed utilizing Eq. (14) with the known distributions of a_x and a_z at the previous instants of time, solved from the TDGL equations discretized in space. We use a uniform mesh of spatial grid points for both the z and x directions, with the discretization intervals equal to $\Delta z = \Delta x = 0.25\, \xi_T(T)$ in all the computations reported in this paper. In each computer simulation, the time step Δt was chosen sufficiently small to ensure an accurate description of the temporal evolution—typically $\Delta t = 0.001\, t_0$, where t_0 is as defined in Eq. (12).

Depending on the current j we obtain different solutions. There exists a critical current j_c (generally a function of w and the applied boundary conditions, D versus S) below which the solutions are stationary and the distributions of ρ_x and ρ_z are homogeneous in z with $\mu = 0$. We discuss our results for the critical currents in Sec. IV.

For $j > j_c$, we find nonstationary nonuniform phase-slip solutions. These have been obtained for several combinations of the channel sizes Lw, with $L = 5$–7 and $w = 5$–25 for diffuse and specular boundary conditions. The qualitative properties of the phase-slip solutions do not depend on the boundary conditions, D versus S.

We shall describe in more detail the phase-slip solutions obtained with the parameter $u = 0.2$ in Eq. (15). We have made several runs with $u = 1$ as well; the results are qualitatively similar.

B. Phase-slip scenarios

For currents $j_c < j < 0.5$, we observe one phase-slip event in both ρ_x and ρ_z per period within L. For the width $w = 5$, the component $a_x = 0$, and a_z oscillates just as for phase slippage in the one-dimensional case.[13] For $w = 6$, the component a_x is finite. Slippages in φ_x and φ_z occur on the line $z = L/2$. The modulus ρ_x vanishes almost simultaneously over the whole width. This suggests a higher-dimensional counterpart of a phase-slip center, a phase-slip line (PSL). Phase slippages in a_z occur via periodic formation and motion of 2π vortices, which nucleate at one side of the channel and move across the flow along $z = L/2$ to the other side, according to the direction of the Magnus force.

Examples of the periodic phase-slip solutions in their limit cycles for a supercritical flow are illustrated in Figs. 4–8 for diffuse and specular boundary conditions for several combinations of the flow-channel dimensions, Lw.

Figures 4 and 5 show the superflow fields $j_z^{(s)} - \langle j_z^{(s)} \rangle$ and $j_x^{(s)}$, and the time-dependent distributions of the chemical potential for the four chosen instants of time [frames (t_1) through (t_4), respectively]. Figure 4 pertains to the channel size $Lw = (6)(10)$ and the current $j = 0.225$ with diffuse boundary conditions, while Fig. 5 is for $Lw = (7)(10)$ and the same current with specular boundaries.

Figure 6 shows distributions of ρ_x and ρ_z for the situation in Fig. 4, while Fig. 7 gives ρ_x and ρ_z for that of Fig. 5. In these figures, one quite clearly observes the formation and motion of a vortex in the a_z component and a PSL in the a_x component; moreover, these scenarios of phase slippage are topologically quite equivalent for both the diffuse and specular boundary conditions.

Figure 8 presents distributions of ρ_x and ρ_z for consecutive instants of time for a broad channel with dimensions $Lw = (7)(25)$ and the current $j = 0.225$. Boundary con-

ditions are diffuse. For such a wide channel we observe vortices in both components, a_x and a_z.

In the course of the passage of a vortex, see Figs. (4) and (5), the magnitude of the chemical-potential difference $|\mu(L)|$ is larger than in the absence of a quantized vortex (t_4), since a higher pressure is required to balance the friction force acting on the moving vortex. At the time when the vortex is passing, the net superflow is decreased; it can even reverse itself, the main current being carried by the normal component.

The formation and motion of a vortex repeats periodically. For example, for w, L, and j, as in Figs. 4 and 6, the period is 7.2 in the time scale (t_0) of Eq. (2). When the current approaches the critical threshold value j_c, the period increases as is commonplace for critical slowing down in general.

Figures 9(a) and 9(b) present hodographs at several points in the channel for the cases depicted in Figs. 4 and 6, and 5 and 7, respectively. A slippage in phase occurs where the trajectory first encircles the origin in the $\mathrm{Im}(a_{x,z})$ versus $\mathrm{Re}(a_{x,z})$ plane. It follows from Figs. 9(a) and 9(b) that the phase slippages for both components occur on the line $z = L/2$.

Since, owing to symmetry, the conditions in Eqs. (22)–(24) are fulfilled also for the line $z = L/2$, the values of the phases φ_x and φ_z on this line are proportional to time. Therefore, different slopes of the trajectories of one component at the origin for varying x on the line $z = L/2$ indicate that the corresponding phase undergoes slippages for different times at these values of x. In Figs. 9(a) and 9(b), we see that the slopes of the trajectories for a_z at the origin are different for varying x, thus indicating that there is a moving vortex. The slopes of the a_x trajectories, on the other hand, are almost equal for different x, which means that a PSL occurs.

C. Breaking of reflection symmetry

The a_z vortex in Figs. 6 and 7 is nucleated at $x = +w/2$, and it moves towards negative x. This behavior

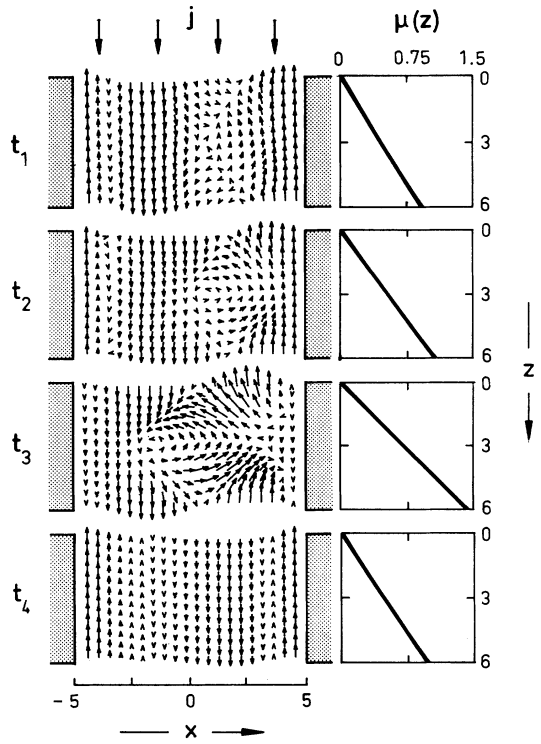

FIG. 4. Superflow patterns ($\mathbf{j}_s$, small arrows) and the simultaneous distributions of chemical potential μ along z for the instants of vortex formation (t_1), vortex motion (t_2 and t_3), and for the vortex-free state (t_4). Current $j_z = 0.225$, the flow-channel dimensions are $w = 10$ and $L = 6$; boundary conditions at the side walls are diffuse. [Figures 6 and 9(a) also correspond to this case.] During the passage of a vortex and just after it, the chemical potential $|\mu(L)|$ is larger than in the absence of vorticity, since a large value of $|\mu|$ is required to balance the friction experienced by the vortex. The frames are for the time instants $t_2 = t_1 + t_0$, $t_3 = t_1 + 1.5\,t_0$, and $t_4 = t_1 + 2\,t_0$. The sequence repeats itself with the period $7.2\,t_0$.

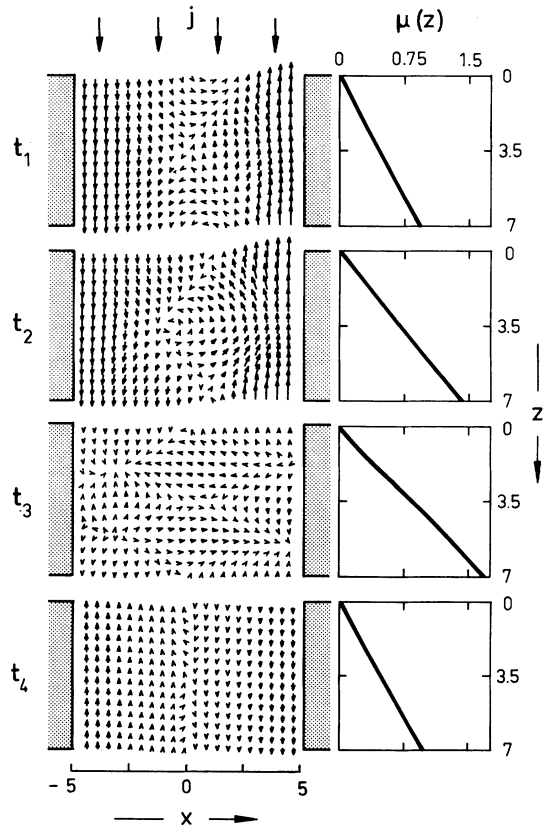

FIG. 5. Same as in Fig. 4, but for specular boundary conditions and channel dimensions $w = 10$ and $L = 7$. Current $j_z = 0.225$; note that the scenario is just the same as in Fig. 4. The time instants are $t_2 = t_1 + 0.5\,t_0$, $t_3 = t_1 + 0.75\,t_0$, and $t_4 = t_1 + 1.25\,t_0$; the period is $13.6\,t_0$. [Figures 7 and 9(b) also correspond to this case.]

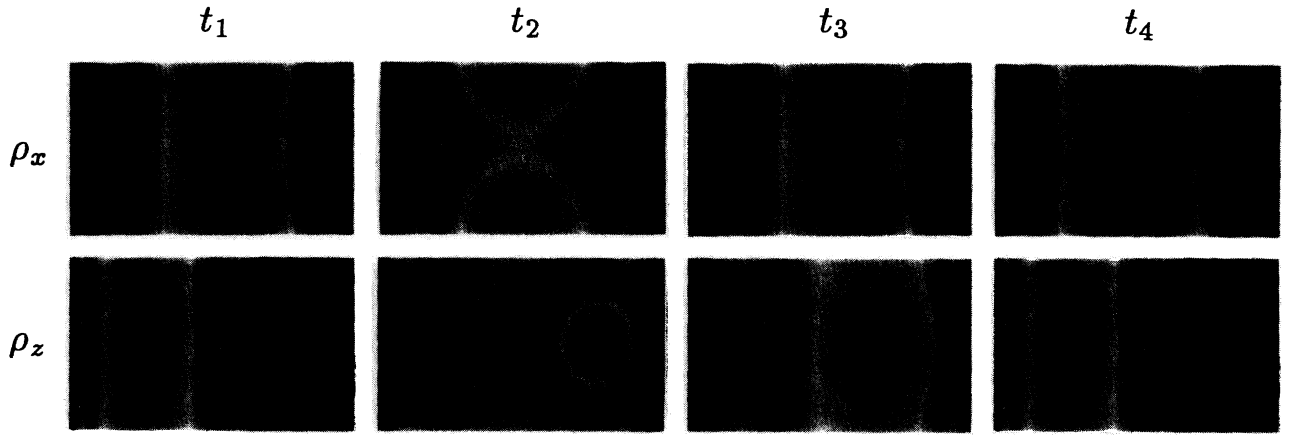

FIG. 6. Computed time evolution for the superfluid amplitudes $\rho_x(z,x;t)$ and $\rho_z(z,x;t)$ for the same time instants and values of all parameters as in Fig. 4. The boundary conditions at the side walls ($x = \pm w/2$) are diffuse. For the amplitudes ρ_x, one sees a strong suppression, which develops into a phase-slip line (PSL) at t_3. For the amplitude ρ_x, we observe a vortex created at the right wall and moving towards left. At t_1, it is just to the left (black spot) from the amplitude maximum indicated by the brighter spot in the very right part of the frame. At t_2 it has moved to the center of the channel, and vanishes to the right wall at t_3. At t_4 the order-parameter distribution has returned to the initial state. (For the grayscale code of the order-parameter amplitudes in Figs. 6, 7, and 8, see the inset on top of Fig. 8.)

corresponds to $k = 0$ in Eq. (22). For $k = 1$, a vortex with the opposite sign of circulation is nucleated at the opposite side of the channel ($x = -w/2$), and it moves towards positive x.

This can be explained by the breaking of reflection symmetry in $x \to -x$; there exists a preferred direction defined by the vector product $\boldsymbol{l} \times \mathbf{j}$ for vortex motion. In unison with surface tension, this gives a contribution to the free energy that is proportional to $\mathbf{n} \cdot \boldsymbol{l} \times \mathbf{j}$, where $\mathbf{n}$ is the wall normal.

In terms of the TDGL equations this symmetry breaking can be understood if we consider the equation for ρ_z on the line $z = L/2$, where conditions (22)–(24) are satisfied. We have

$$u\frac{\partial \rho_z}{\partial t} = \rho_z + 3\left[\frac{\partial^2 \rho_z}{\partial z^2} - \left(\frac{\partial \varphi_z}{\partial z}\right)^2 \rho_z\right] + \frac{\partial^2 \rho_z}{\partial x^2} - (3\rho_z^3 + \rho_z \rho_x^2) + 2\left(\frac{\partial \varphi_x}{\partial x}\frac{\partial \rho_x}{\partial x} + \frac{\partial^2 \varphi_x}{\partial x \partial z}\rho_z\right)\sin(\varphi_z - \varphi_x). \tag{27}$$

For even k, the final term in Eq. (27) is positive at $x = -w/2$, but negative for $x = +w/2$, owing to the sign of $\partial \rho_x / \partial x$, since $\rho_x = 0$ at $x = \pm w/2$. Consequently, a vortex can be nucleated more easily for $x = +w/2$. For

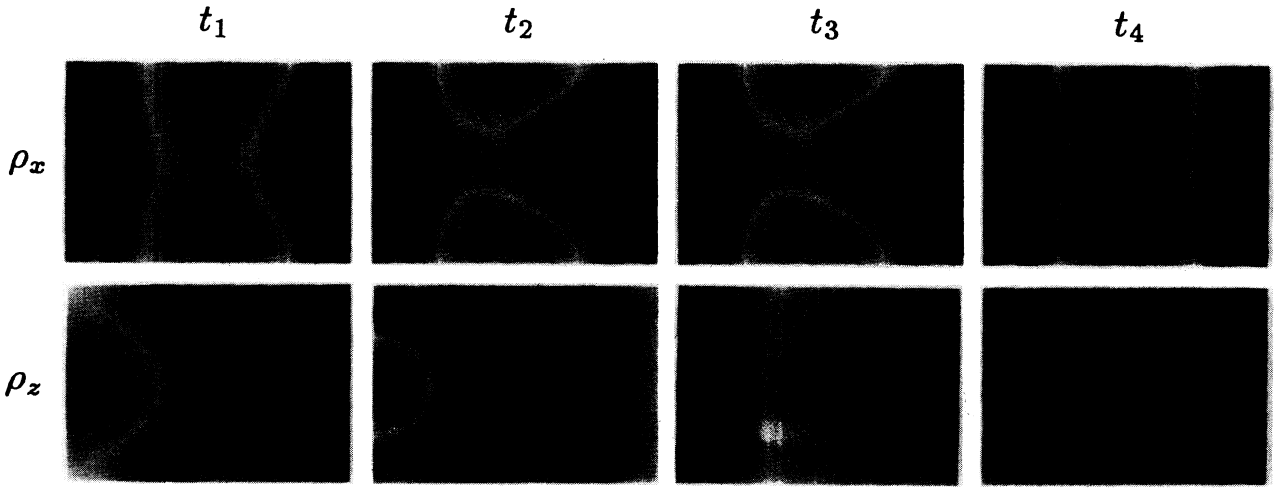

FIG. 7. Time evolution of the amplitudes $\rho_x(z,x;t)$ and $\rho_z(z,x;t)$ for the same values of parameters as in Fig. 5. Boundary conditions are specular. One sees a phase-slip line in the component ρ_x, and a vortex (black spot) moving towards left in the component ρ_z, just as in the case of diffuse boundary conditions of Fig. 6.

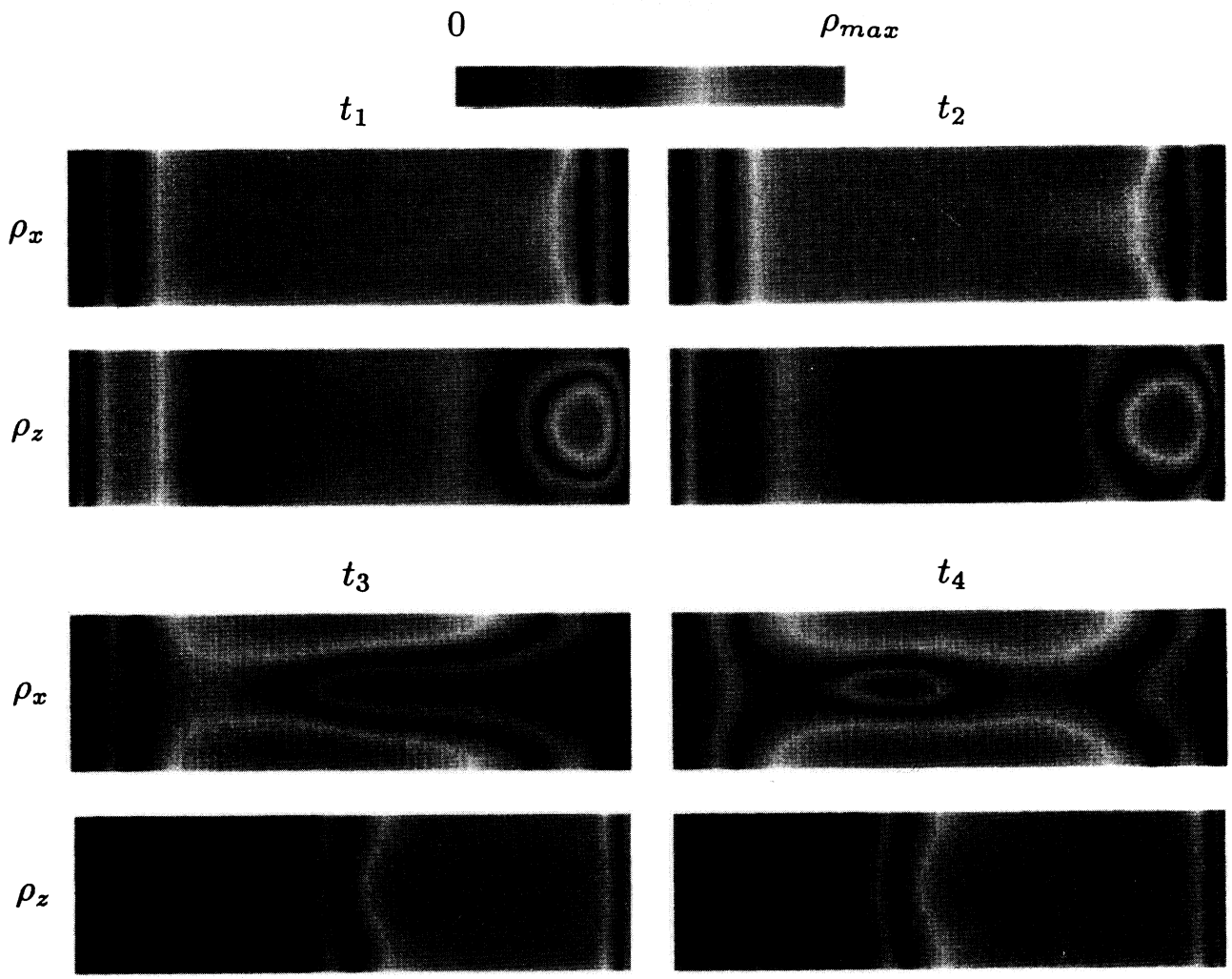

FIG. 8. Time evolution of $\rho_x(z,x;t)$ and $\rho_z(z,x;t)$ as in Figs. 6 and 7, but for a very wide channel with $w = 25$, $L = 7$; diffuse boundary conditions are applied. Here the period is $10t_0$; the frames are taken at $t_2 = t_1 + 0.5\,t_0$, $t_3 = t_1 + 2.5\,t_0$, and $t_4 = t_1 + 2.5\,t_0$. A grayscale value is assigned to the amplitudes according to the code given at the top of the figure. At t_1 there is a vortex in the ρ_z component (the suppression denoted by the black spot close to the right wall). At t_2 the vortex has moved toward the left wall and a suppression of the ρ_z component in the middle of the channel has occurred. At t_3 a vortex is formed in the ρ_x component, which at t_4 has moved towards the left wall. Note that now both the components relax via formation and motion of vortex structure.

odd k, the vortex nucleates at $x = -w/2$, instead.

Comparing Figs. 6 and 7 with Fig. 8, we observe different types of phase-slip processes depending on the channel width. There can be phase-slip lines or vortices in one or in both components of the order parameter. These are finite-size effects due to the channel width: if the solution for ρ_x has to satisfy the boundary conditions $\rho_x = 0$ at $x = \pm w/2$, and also the condition $\rho_x = 0$ at $x = 0$ due to an a_x vortex in the middle of the channel, the order-parameter component will have a very small amplitude for small w. This results in the formation of a PSL instead of a vortex in the a_x component. The effect of a finite w on the a_z component is less prominent, since there is no factor of 3 in the corresponding spatial derivative terms for gradient energy.

The size effects due to finite L are observed in the a_z component. For $L = 5$, vortex formation in a_z is accompanied by a substantial suppression of ρ_z on the line $x \simeq$ const, passing through the vortex along the channel (a "laminar structure"). For the larger $L = 6$ and 7, this effect is less pronounced. The suppression of ρ_z is stronger on the background of the more developed component ρ_x, as can be verified in comparing Figs. 6 and 8.

IV. DISCUSSION

A. Critical currents for vortex nucleation

The results obtained from extensive numerical computations for the critical current as a function of w for D and S boundary conditions are collected in Fig. 10.

An analysis of the stationary solutions of Eqs. (14) and (15) for low currents shows that for the very wide channels, with $w \to \infty$, for which the distributions of ρ_x and ρ_z can be considered uniform over x and z, one has

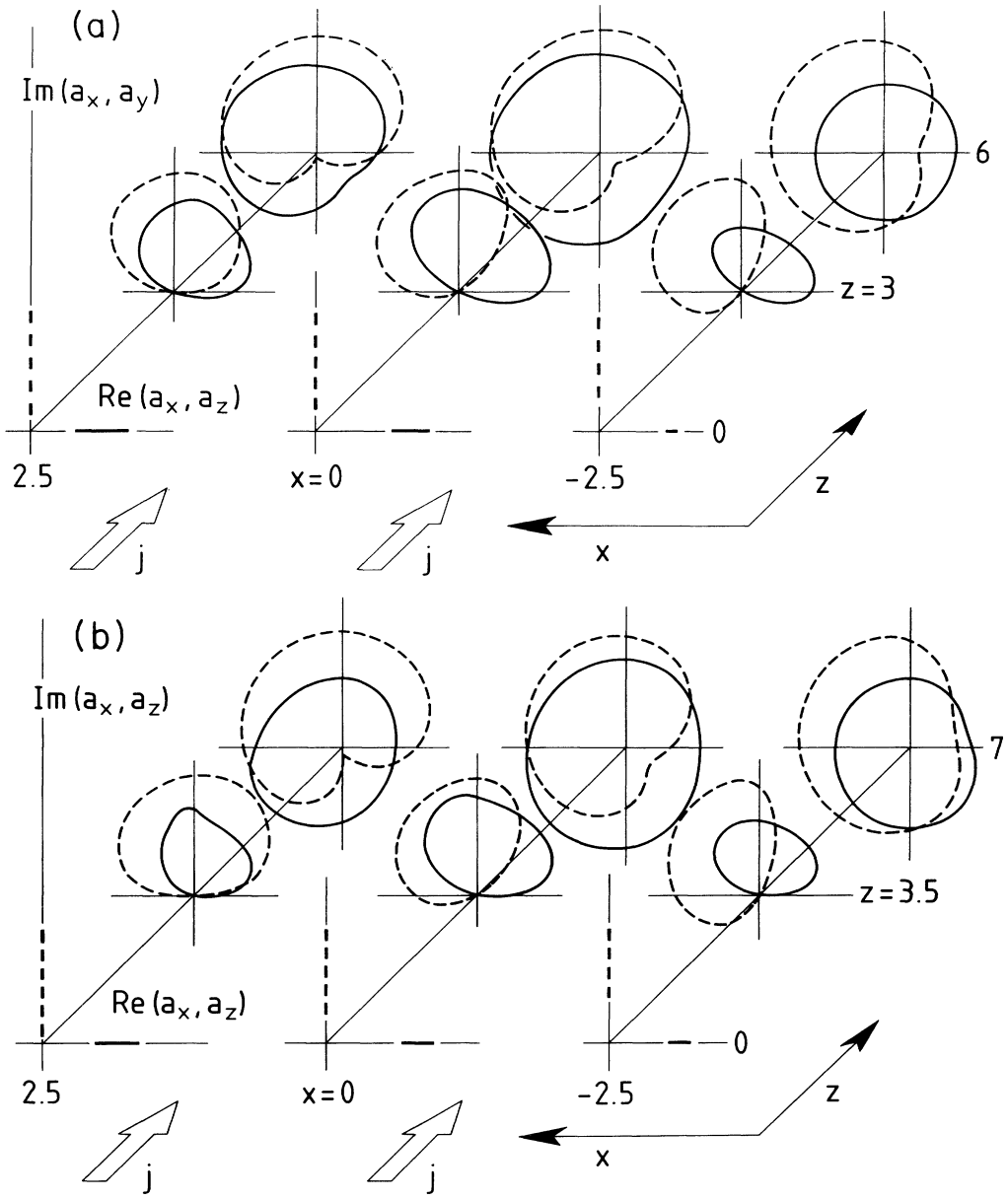

FIG. 9. Hodographs for the amplitudes a_x (full lines) and a_z (dashed) at different positions (z,x) in the two-dimensional flow field. (a) For the diffuse case (Figs. 4 and 6), and (b) for the specular case (Figs. 5 and 7). Orbits for both a_x and a_z at $z = L$ encircle the origin once, indicating phase slippage by 2π. The hodographs evolve gradually along z; they first develop small loops that touch the origin at $z = L/2$, thus locating the phase-slip events for each component to the middle of the flow channel.

$$\rho_x = \tfrac{1}{2}\,, \quad \rho_z = \sqrt{\tfrac{1}{4} - q^2}\,, \tag{28}$$

where $\partial\varphi_z/\partial z = \partial\varphi_x/\partial z = q$. Equation (28) applies to both specular and diffuse boundary conditions, since the depressions of ρ_x and ρ_z near the walls give only negligible corrections. The supercurrent $j_z^{(s)} = q - 3q^3$ has the maximum value

$$j_c = \tfrac{2}{9}. \tag{29}$$

This coincides with the result of Fetter and Ullah,[26] with the proper choice for the order-parameter normalization.

For a finite width, superfluidity is preserved down to $w \to 0$ in the case of specular boundary conditions. For small w there exists polar phase with $\rho_x = 0$ and constant ρ_x. Also in this case one finds $j_c = \frac{2}{9}$.

For diffuse boundary conditions at the side walls, superfluidity in the channel and the critical current vanish for $w = \pi$. With $w \to \pi$, the maximum averaged supercurrent density is

$$j_c = \langle j_z^{(s)} \rangle_{\max} = \frac{8\sqrt{2}}{3\sqrt{3}} \left(\frac{w - \pi}{\pi} \right)^{3/2}. \tag{30}$$

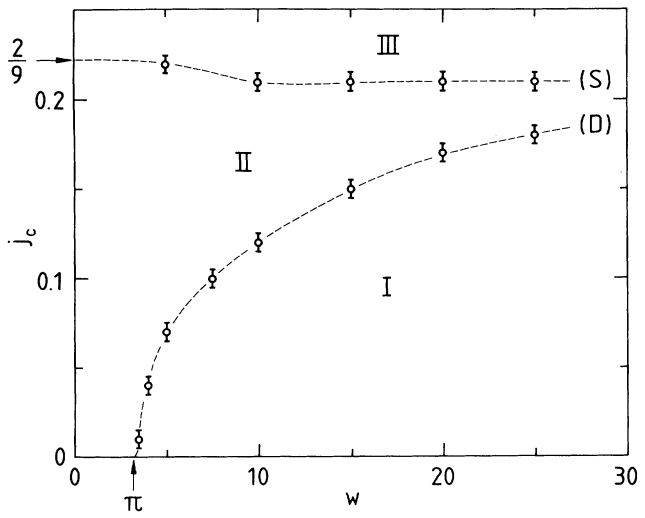

FIG. 10. Calculated critical currents j_c [in units of j_0, defined by Eq. (11)] for the diffuse (D) and specular (S) boundary conditions as functions of w, the width of the channel [in units of $\xi_T(T)$, defined by Eq. (10)]. The circles indicate the critical current obtained as the mean value of two currents, such that the solution of the TDGL equations is stationary for the lower current, while it exhibits phase slippages for the higher current; the vertical bars denote the interval between the two currents. Line (D) indicates that in region I the solution for the diffuse case is stationary, while in region II phase-slip solutions are encountered. Correspondingly, curve (S) demarcates the regimes of stationary and periodic (region III) solutions for the specular boundary conditions.

The circles in Fig. 10 display the values for the critical current j_c obtained by direct numerical solution of the dynamic equations (13)–(15). For j_c at each w, we take the mean value of two neighboring currents j_{c_1} and j_{c_2} ($j_{c_2} > j_{c_1}$), such that the solution remains stationary for $j = j_{c_1}$, while it is nonstationary already for j_{c_2}. The error bars in Fig. 10 indicate the intervals between j_{c_2} and j_{c_1}.

For specular boundary conditions, there exists a minimum in j_c as a function of w due to a transition from the polar phase with $\rho_z = \text{const}$ to the A phase with a nonuniform distribution of ρ_x. The critical current initially decreases with increasing w; it then seems to increase slowly, which can be seen from the fact that the time period of phase-slip oscillations at $j = j_{c_2}$ increases, thus indicating a decrease in the normal current. The critical current seems to saturate for both specular and diffuse conditions with further increase in w. Note that the critical current for the vortex nucleation in wide channels need not coincide with the bulk pair-breaking current because of the effects of walls which may promote the formation of vortices.

B. Models for vortex nucleation

It is interesting to relate our results for the critical current with known models of vortex nucleation in superfluids.[8,27] When superfluid helium is flowing through channels having relatively large cross sections of characteristic transverse size R, friction arises at quite low flow velocities. It is supposed that dissipation is produced by the moving vortices and that it begins when the flow velocity exceeds the critical velocity introduced by Feynman:[28]

$$v_{\text{Feynman}} \propto \frac{\hbar}{mR} \ln\left(\frac{R}{\xi}\right) . \tag{31}$$

This critical velocity indicates when vortices can exist in the channel; the other aspect of the problem is how they can be created there in the first place. One possibility is the nucleation of vortices at the walls of the channel. However, the presence of the surface-energy barrier hinders the nucleation of vortices.

In superfluid He II, this barrier can be lowered by surface roughness; this promotes the formation of small vortex loops,[29] which then can grow, for example, due to thermal activation.[30] The surface barrier may also be overcome by quantum tunneling. In superfluid ^{3}He, surface roughness also promotes vortex formation, since it suppresses the order-parameter components near the walls, thus decreasing the energy barrier. For a smooth surface, however, the barrier is very high at low velocities, especially as it is to be compared with the much lower temperatures pertaining to the existence of superfluidity in ^{3}He.

According to the theory of vortex nucleation in He II of Ref. 31, which can also be applied to superfluid ^{3}He, the energy per unit length of a quantized vortex line due to its interactions with the wall and with the superfluid flow is, in order of magnitude,

$$E = \frac{\pi\hbar^2\rho_s}{4m^2}\left(\ln\frac{x+\xi}{\xi} - \frac{4mxv_s}{\hbar}\right) , \tag{32}$$

where x is the distance between the vortex and the wall, ξ is the vortex-core size, and v_s is the flow velocity. Equation (32) applies to a single-quantum vortex with the "superfluid particle" mass $2m$. The first term is due to the attraction of the vortex to the wall, while the second one describes the interaction between the vortex and the flow (the Magnus force). The limit for the validity of Eq. (32) is $x \gg \xi$. However, it may be used as an interpolation down to $x \simeq \xi$, since it accounts for the vanishing of energy as $x \to 0$. The energy barrier is [i.e., the maximum of Eq. (32) as a function of x]:

$$E_{\max} = \frac{\pi\hbar^2\rho_s}{4m^2}\left(\ln\frac{v_c}{v} - 1 + \frac{v}{v_c}\right) ; \tag{33}$$

$E_{\max}$ vanishes at $v = v_c$, where

$$v_c \simeq \frac{\hbar}{4m\xi} . \tag{34}$$

This is the critical velocity at which vortices are spontaneously formed off the walls of the channel. It differs from Eq. (31); however, these two critical velocities agree in their order of magnitude for channel sizes $R \simeq \xi$.

In He II, where ξ is small, the critical velocity in Eq. (34) is very high. However, v_c for ^{3}He is much lower and can be attained rather easily experimentally. For sin-

gular vortices with $\xi \approx \xi(T)$, the order of magnitude for the critical velocity is the pair-breaking velocity (about 10 cm/sec), which is independent of the channel size.

For continuous vortices in ^{3}He-A, the vortex-core size ξ is considerably larger and can be even on the order of the channel size, R, and hence the critical velocity is considerably diminished. This conclusion agrees well with the experimental observation[32] that it is very difficult to produce singular vortices in the B phase by rotating the container, unless the velocity of rotation is quite high, whereas continuous vortices in the A phase can be produced easily.

These simple arguments for the critical velocity of spontaneous vortex formation (see also Refs. 1, 28, and 33), well agree with the results of our numerical computations for the critical current. The data in Fig. 10 yields directly the value of the current above which there appears an instability against vortex formation. The critical current saturates for large w, in agreement with the observation that the critical velocity (34) for the nucleation of vortices with core radii on the order of $\xi(T)$ does not depend on the channel size.

C. Superfluid-core vortices

We have found various types of phase-slip processes depending on the channel width w. For small w, vortices in ρ_z occur in conjuction with phase-slip lines for ρ_x. For wider channels ($w > 15$) we observe vortices in both components. One can describe the solutions in terms of a global order-parameter phase, φ, defined, for example, as $\varphi = \varphi_z(L)$, since the phase difference $\varphi_z - \varphi_x$ is fixed for $z = L$. The phase-slip solutions of both types are equivalent to 2π vortices in φ passing across the channel: the global phase φ relaxes through 2π after each phase-slip event, as can be verified with help of the hodographs in Figs. 9(a) and 9(b).

A characteristic feature of the phase-slip solutions obtained is that even though the phase slippage for each component takes place on the line $z = L/2$, the points where $\rho_{x,z} = 0$ never coincide, except for the possible situation when a vortex in one component (or a PSL) catches up a vortex in the other one.

This can be seen in particular from the hodographs in Figs. 9. On the line $z = L/2$ the trajectories in the origin intersect each other at different angles for varying x; therefore, the phase slippages in both components take place through different time intervals for the corresponding x.

In other words, the vortices obtained have superfluid cores, despite the fact that the $\boldsymbol{l}$ vector is fixed. In contrast to the continuous vortices in the A phase with even number of circulation quanta, these singularities are singly quantized. This does not contradict the general topological classification[34] of defects in superfluid ^{3}He, since here the superfluid vortex cores are on the order of the coherence length, $\xi(T)$. The momentum-space topology of these vortices is similar to that for phase-slip centers in the one-dimensional flow.[35]

First experiments on phase slippage in superfluid ^{3}He-A have been reported recently.[36] In these experiments, it seems highly probable that the microscopic state of the superfluid in the weak link is fixed locally by the presence of the walls; this conforms with our model for the flow channel, see Fig. 3(a). These experiments were conducted at 28.4 bars; they produced a staircase pattern analogous to that first found in He II. The staircase structure may be associated with the appearance of new lines across the channel along which vortices are traversing.

In our numerical simulation, the pressure difference between the ends of the channel increases during the passage of a vortex and then relaxes to the value determined by the difference $j - j_c$. This situation differs from that in the experiment,[6] where the pressure at the channel ends was kept constant. The approach used in the present paper can be applied also for the problem with a given pressure difference, the results are planned to be published elsewhere.

D. Summary

We have considered vortex formation in a channel under a fixed total current of ^{3}He flowing through it; we have confirmed Anderson's scenario[2] for superfluid phase slippage through the traversal of quantized vortex lines.

In conclusion, we have studied the formation and structure of vortices in two-dimensional flow of superfluid ^{3}He-A through a channel with transverse dimensions on the order of the coherence length, using computer simulations of time-dependent Ginzburg-Landau equations. Depending on the channel width, phase-slip processes in the two-component order parameter for ^{3}He-A can take place via the formation of vortices or phase-slip lines in one or both components of the order parameter. The phase-slip objects generated are singly quantized superfluid-core vortices with a fixed orientation of the $\boldsymbol{l}$ vector, in contrast to the continuous vortices in bulk superfuid ^{3}He-A.

Phase coherence in superfluids and superconductors is a fundamental physical property, which arises from the very existence of a macroscopic quantum-mechanical order-parameter field reflecting the broken gauge symmetry. The order parameter in superfluid ^{3}He possesses a particularly rich multicomponent structure; it may prove useful for corresponding investigations of high-temperature, heavy-fermion, and other novel superconductors exemplifying exotic pairing and exhibiting nontrivial superconducting order parameters with internal degrees of freedom.

ACKNOWLEDGMENTS

We are grateful to I. M. Khalatnikov, M. Krusius, J. P. Pekola, and G. E. Volovik for stimulating discussions, to O. V. Lounasmaa for useful comments on the manuscript, and to O. Avenel and E. Varoquaux for their interest. The CPU-intensive computer simulations were performed at the Finnish Centre for Scien-

tific Computing; the assistance of the staff there, special thanks are due to R. M. Nieminen, is gratefully acknowledged. Figures 6, 7, and 8 were produced with help of the public-domain program NCSA IMAGE. Research supported through funds for the Advancement of European Science by the Körber-Stiftung (Hamburg, Germany) and by the Soviet Academy of Sciences and the Academy of Finland through the project ROTA.

---

*Permanent address: L. D. Landau Institute for Theoretical Physics, U.S.S.R. Academy of Sciences, 117334 Moscow, U.S.S.R.

†Present address: Institut für Theorie der Kondensierten Materie, Universität Karlsruhe (TH), D-7500 Karlsruhe 1, Germany.

[1] R. J. Donnelly, *Quantized Vortices in Helium II* (Cambridge University Press, Cambridge, 1991).

[2] P. W. Anderson, Rev. Mod. Phys. **38**, 298 (1966).

[3] D. N. Paulson, M. Krusius, and J. C. Wheatley, Phys. Rev. Lett. **37**, 599 (1976).

[4] G. E. Volovik, Pis'ma Zh. Eksp. Teor. Fiz. **27**, 573 (1978) [JETP Lett. **27**, 605 (1978)].

[5] T.-L. Ho, Phys. Rev. Lett. **41**, 1473 (1978).

[6] O. Avenel and E. Varoquaux, Phys. Rev. Lett. **60**, 416 (1988).

[7] A. L. Fetter, in Prog. Low Temp. Phys., edited by D. F. Brewer (North-Holland, Amsterdam, 1986), Vol. X, p. 1.

[8] D. Vollhardt and P. Wölfle, *The Superfluid Phases of Helium 3* (Taylor & Francis, London, 1990).

[9] R. C. M. Dow and J. R. Hook, Phys. Rev. Lett. **55**, 2305 (1985).

[10] A. L. Fetter, J. Low Temp. Phys. **70**, 499 (1988).

[11] M. M. Salomaa and G. E. Volovik, Phys. Rev. Lett. **51**, 2040 (1983); Phys. Rev. B **31**, 203 (1985).

[12] P. I. Soininen, N. B. Kopnin, and M. M. Salomaa, Europhys. Lett. **14**, 49 (1991); N. B. Kopnin, P. I. Soininen, and M. M. Salomaa, Physica B **169**, 535 (1991).

[13] N. B. Kopnin and M. M. Salomaa, Phys. Rev. B **41**, 2601 (1990).

[14] B. I. Ivlev and N. B. Kopnin, Adv. Phys. **33**, 47 (1984).

[15] L. Kramer (private communication); A. Weber and L. Kramer (unpublished).

[16] H. Monien and L. Tewordt, J. Low Temp. Phys. **62**, 277 (1986); E. V. Thuneberg, Europhys. Lett. **7**, 441 (1988).

[17] I. M. Khalatnikov, *An Introduction to the Theory of Superfluidity* (Benjamin, Reading, MA, 1965).

[18] V. Ambegaokar, P. G. deGennes, and D. Rainer, Phys. Rev. A **9**, 2676 (1974); **12**, 345(E) (1975).

[19] E. M. Lifshitz and L. P. Pitaevskiĭ, *Physical Kinetics* (Pergamon, Oxford, 1981).

[20] J. C. Wheatley, Rev. Mod. Phys. **47**, 415 (1975).

[21] L. P. Gor'kov and G. M. Eliashberg, Zh. Eksp. Teor. Fiz. **54**, 612 (1968) [Sov. Phys. JETP **27**, 328 (1968)].

[22] L. H. Kjäldman, J. Kurkijärvi, and D. Rainer, J. Low Temp. Phys. **33**, 577 (1978).

[23] N. B. Kopnin, J. Low Temp. Phys. **65**, 433 (1986).

[24] M. T. Manninen and J. P. Pekola, J. Low Temp. Phys. **52**, 497 (1983); J. P. Pekola, J. C. Davis, Zhu Yu-Qun, R. N. R. Spohr, P. B. Price, and R. E. Packard, *ibid.* **67**, 47 (1987).

[25] R. J. Watts-Tobin, Y. Krähenbühl, and L. Kramer, J. Low Temp. Phys. **42**, 459 (1981).

[26] A. L. Fetter and S. Ullah, J. Low Temp. Phys. **70**, 515 (1988).

[27] P. Nozières and D. Pines, *The Theory of Quantum Liquids Vol. II: The Superfluid Bose Liquids* (Addison-Wesley, Menlo Park, 1990).

[28] R. P. Feynman, in Prog. Low Temp. Phys., edited by C. J. Gorter (North-Holland, Amsterdam, 1964), Vol. I, p. 17.

[29] G. E. Volovik, Pis'ma Zh. Eksp. Teor. Fiz. **15**, 116 (1972) [JETP Lett. **15**, 81 (1972)].

[30] S. V. Iordanskiĭ, Zh. Eksp. Teor. Fiz. **48**, 708 (1965) [Sov. Phys. JETP **21**, 467 (1965)].

[31] C. M. Muirhead, W. F. Vinen, and R. J. Donnelly, Philos. Trans. R. Soc. London, Ser. A **311**, 433 (1984).

[32] P. J. Hakonen and K. K. Nummila, Phys. Rev. Lett. **59**, 1006 (1987); M. M. Salomaa, J. Phys.: Condens. Matter **2**, 1325 (1990); J. S. Korhonen, A. D. Gongadze, Z. Janu, Y. Kondo, M. Krusius, Yu. M. Mukharsky, and E. V. Thuneberg, Phys. Rev. Lett. **65**, 1211 (1990).

[33] E. Varoquaux, W. Zimmerman, Jr., and O. Avenel, (unpublished).

[34] G. E. Volovik and V. P. Mineev, Zh. Eksp. Teor. Fiz. **72**, 2256 (1977) [Sov. Phys. JETP **45**, 1186 (1977)].

[35] N. B. Kopnin and M. M. Salomaa, Physica B **165+166**, 629 (1990).

[36] O. Avenel and E. Varoquaux, in *Quantum Fluids and Solids (Gainesville, 1989*, Proceedings of the Conference on Quantum Fluids and Solids, AIP, Conf. Proc. **194**, edited by G. G. Ihas and Y. Takano (AIP, New York, 1989), p. 3.

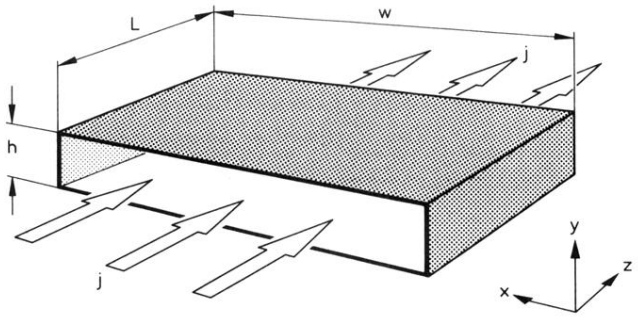

FIG. 1. Schematic illustration for the model "matchbox" geometry of the superfluid ^{3}He flow channel considered in this paper. In order to correspond to available experiments, the channel is here taken to be a wide rectangular slit of height h, width w, and length L. In the numerical simulations, a total constant current j (indicated by the large arrows in this figure) is imposed along z.

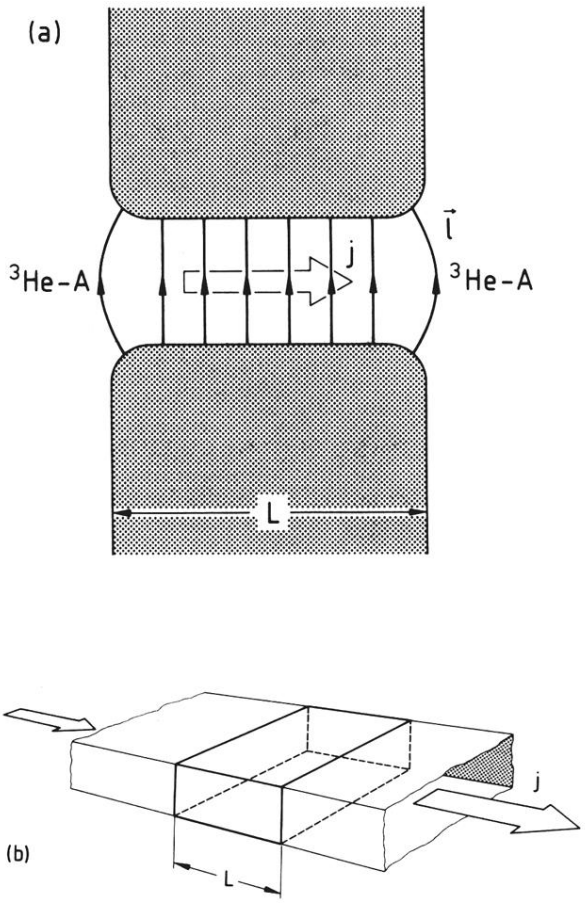

FIG. 3. Experimental physical realizations of the flow geometry considered: (a) a slit of length L, connecting two vessels of superfluid ^{3}He-A; solid arrows display the l-vector texture, open arrow represents the current flow, j; (b) a section, having length L, of a long flow channel with the current j passing through. Boundary conditions are periodic along the flow field.

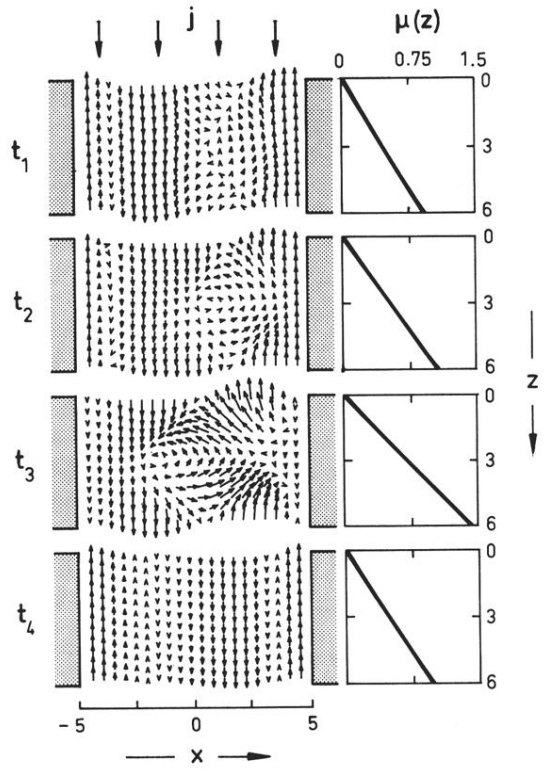

FIG. 4. Superflow patterns ($\mathbf{j}_s$, small arrows) and the simultaneous distributions of chemical potential μ along z for the instants of vortex formation (t_1), vortex motion (t_2 and t_3), and for the vortex-free state (t_4). Current $j_z = 0.225$, the flow-channel dimensions are $w = 10$ and $L = 6$; boundary conditions at the side walls are diffuse. [Figures 6 and 9(a) also correspond to this case.] During the passage of a vortex and just after it, the chemical potential $|\mu(L)|$ is larger than in the absence of vorticity, since a large value of $|\mu|$ is required to balance the friction experienced by the vortex. The frames are for the time instants $t_2 = t_1 + t_0$, $t_3 = t_1 + 1.5\,t_0$, and $t_4 = t_1 + 2\,t_0$. The sequence repeats itself with the period $7.2\,t_0$.

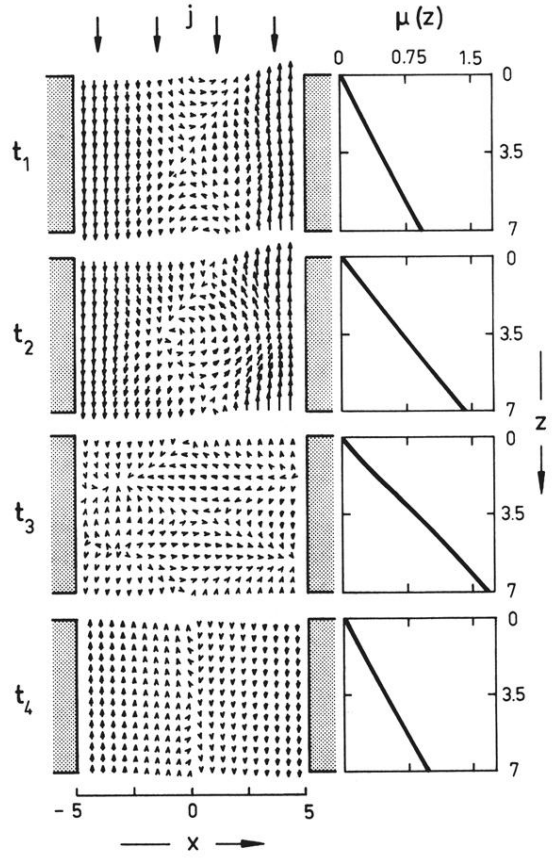

FIG. 5. Same as in Fig. 4, but for specular boundary conditions and channel dimensions $w = 10$ and $L = 7$. Current $j_z = 0.225$; note that the scenario is just the same as in Fig. 4. The time instants are $t_2 = t_1 + 0.5\,t_0$, $t_3 = t_1 + 0.75\,t_0$, and $t_4 = t_1 + 1.25\,t_0$; the period is $13.6\,t_0$. [Figures 7 and 9(b) also correspond to this case.]

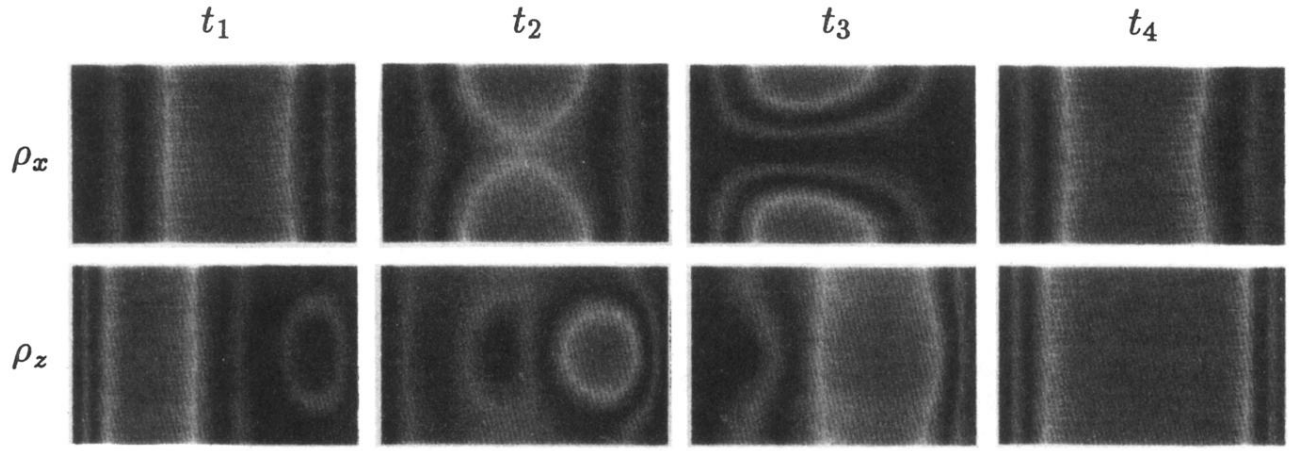

FIG. 6. Computed time evolution for the superfluid amplitudes $\rho_x(z,x;t)$ and $\rho_z(z,x;t)$ for the same time instants and values of all parameters as in Fig. 4. The boundary conditions at the side walls ($x = \pm w/2$) are diffuse. For the amplitudes ρ_x, one sees a strong suppression, which develops into a phase-slip line (PSL) at t_3. For the amplitude ρ_x, we observe a vortex created at the right wall and moving towards left. At t_1, it is just to the left (black spot) from the amplitude maximum indicated by the brighter spot in the very right part of the frame. At t_2 it has moved to the center of the channel, and vanishes to the right wall at t_3. At t_4 the order-parameter distribution has returned to the initial state. (For the grayscale code of the order-parameter amplitudes in Figs. 6, 7, and 8, see the inset on top of Fig. 8.)

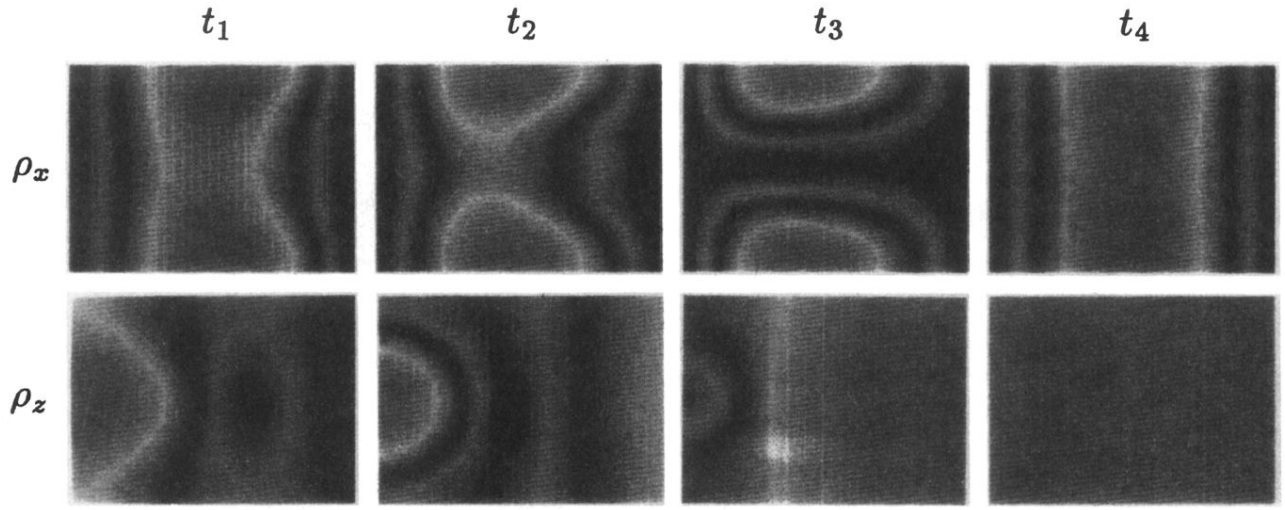

FIG. 7. Time evolution of the amplitudes $\rho_x(z,x;t)$ and $\rho_z(z,x;t)$ for the same values of parameters as in Fig. 5. Boundary conditions are specular. One sees a phase-slip line in the component ρ_x, and a vortex (black spot) moving towards left in the component ρ_z, just as in the case of diffuse boundary conditions of Fig. 6.

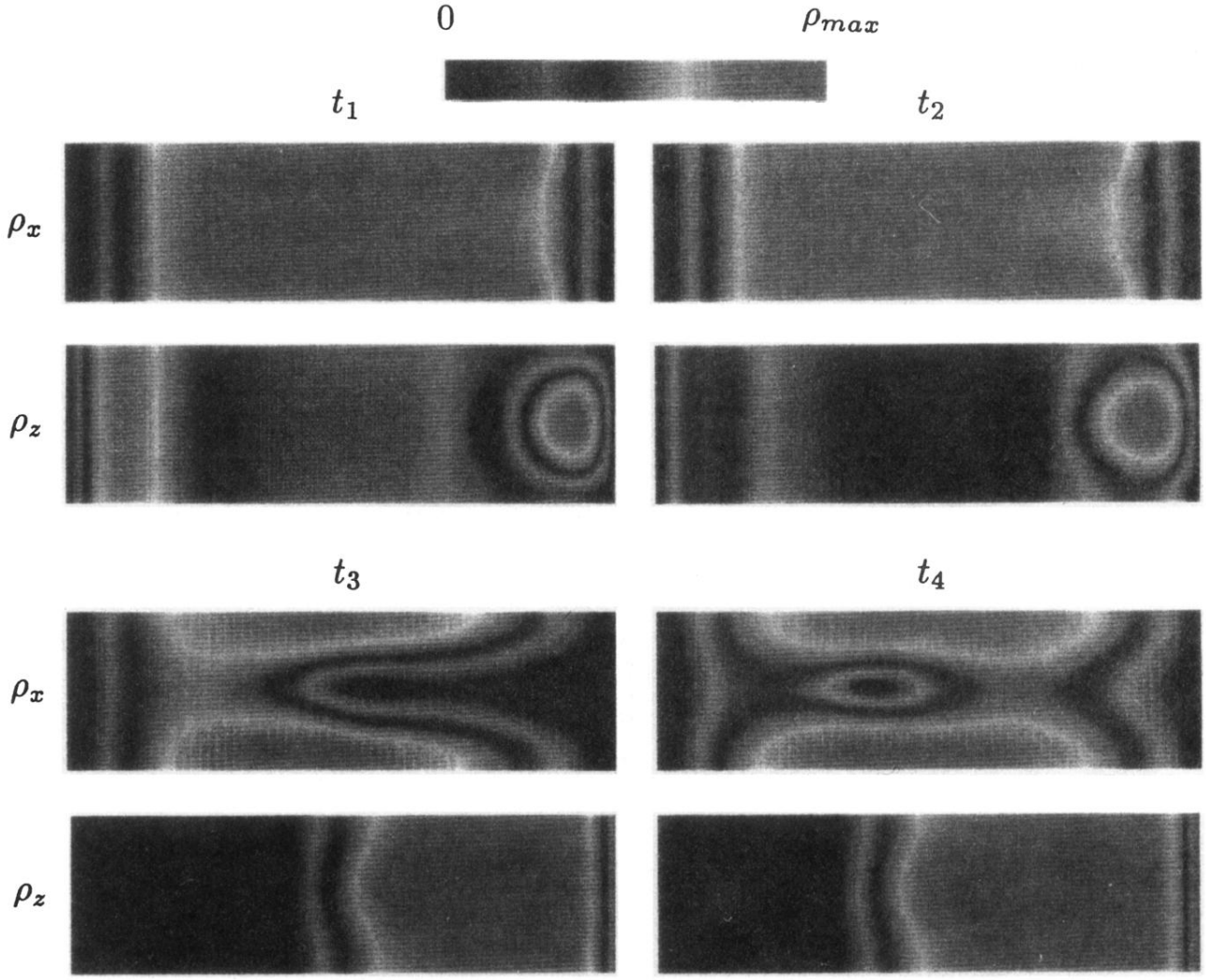

FIG. 8. Time evolution of $\rho_x(z,x;t)$ and $\rho_z(z,x;t)$ as in Figs. 6 and 7, but for a very wide channel with $w = 25$, $L = 7$; diffuse boundary conditions are applied. Here the period is $10t_0$; the frames are taken at $t_2 = t_1 + 0.5\,t_0$, $t_3 = t_1 + 2.5\,t_0$, and $t_4 = t_1 + 2.5\,t_0$. A grayscale value is assigned to the amplitudes according to the code given at the top of the figure. At t_1 there is a vortex in the ρ_z component (the suppression denoted by the black spot close to the right wall). At t_2 the vortex has moved toward the left wall and a suppression of the ρ_z component in the middle of the channel has occurred. At t_3 a vortex is formed in the ρ_x component, which at t_4 has moved towards the left wall. Note that now both the components relax via formation and motion of vortex structure.